J Therm Anal Calorim (2010) 100:629–639
DOI 10.1007/s10973-009-0545-y

Characterization of polypropylene/layered silicate nanocomposites prepared by single-step method

Luljeta Raka · Gordana Bogoeva-Gaceva · Joachim Loos

Received: 31 March 2009 / Accepted: 7 October 2009 / Published online: 13 January 2010

Abstract The extent of organo-modified clay (C93A) platelets dispersion in polymer matrix and crystallization and melting behavior of iPP-based nanocomposites prepared by a single-step melt-mixing method were investigated by wide-angle X-ray diffraction (WAXD), transmission (TEM), scanning electron microscopy (SEM), and differential scanning calorimetry (DSC). WAXD patterns revealed exfoliated structure of nanocomposites containing 1 wt% clay, and mixed intercalated/exfoliated structure at higher concentration of nanoclay. The isothermal crystallization proceeds faster in the matrix polymer (iPP/PP-*g*-MA) than in nanocomposite samples. The results obtained for T_m^o suggest that the presence of nanoclay has induced a perfection of the formed crystals. The presence of C93A particles in PP leads to increase in crystallization peak temperature implying nucleating ability of clay particles, which was more pronounced in exfoliated than in mixed intercalated/exfoliated system.

Keywords Crystallization · Organo-modified clay · PP · Nanocomposites

L. Raka
Faculty of Natural Sciences and Mathematics, State University of Tetovo, Bul. Ilinden, 1200 Tetovo, R. Macedonia

G. Bogoeva-Gaceva (✉)
Faculty of Technology and Metallurgy, University "Ss. Cyril and Methodius", Rudjer Boskovic 16, 1000 Skopje, R. Macedonia
e-mail: gordana@tmf.ukim.edu.mk

J. Loos
Laboratory of Materials and Interface Chemistry, Eindhoven University of Technology, 5600 MB Eindhoven, The Netherlands

J. Loos
Dutch Polymer Institute, P. O. Box 902, 5600 AX Eindhoven, The Netherlands

J. Loos
Department of Chemical Engineering and Chemistry, Eindhoven University of Technology, P.O. Box 513, 5600 MB Eindhoven, The Netherlands

Introduction

Polymer nanocomposites have received intense research interest over the last decade due to the significant macroscopic material properties enhancement over neat polymers and conventional composites, leading to superior mechanical properties, improved flammability resistance, and barrier properties toward different gases [1–7]. These materials based on nanometer-sized particles dispersed in polymer matrices can be produced by different methods, such as in situ polymerization, solution mixing, melt compounding [8], and, recently developed new latex technique [9, 10].

Among the different nanoparticles used in polymer nanocomposites as reinforcement, layered silicates (clay) have been widely studied primarily because of significant enhancement in properties due to their large aspect ratio [11], negative surface charge (cation-exchange capacity) (CEC), layer morphology, sticky behavior, and swelling characteristics, and are regarded as hydrophobic colloids of the constant-charge type [12, 13].

The properties of polymer/clay nanocomposites (PCN) are greatly affected by the complex mechanism of dispersion of silicate layers into the polymer matrix [14, 15]. The key factors for the preparation of enhanced performance

nanomaterials are a homogeneous distribution of nanoparticles within the polymer matrix, and a strong interfacial adhesion between matrix and nanofiller. Uniform dispersion of the nanometer particles offers a major specific surface area enhancement, compared with conventional reinforcements of micrometer size [16].

Preparation of thermoplastic CNs by melt mixing using extrusion process remains the solution of choice, especially with commodity thermoplastics polyolefins as polypropylenes (PP), which are of great interest for the automotive industry. However, melt-mixed PP-based nanocomposites remain still an important challenge since the complete dispersion of clay in single platelets (exfoliation) has not been successfully achieved yet; the usual result, instead, is rather poor intercalation, where the layered silicate remains in stacks with expanded galleries [17]. The use of coupling agents mainly based on maleic anhydride-grafted PP (PP-*g*-MA), type and content of clay intercalant (clay organic modification), and high coupling agent-to-clay ratio have been shown to significantly improve clay intercalation and its dispersion in a polymer matrix [18].

It should be mentioned that the physical mechanical properties are not the only aspect of this class of polymer-based materials, which undergo changes. The structure of the polymer and its thermal behavior also vary significantly as a consequence of addition of the filler, the compatibilizing and processing agent, as well as interaction between compatibilizing agent and matrix polymer (iPP) [19, 20]. The incorporation of layered silicates acting as effective heterogeneous nucleating agents into polymer matrix could impact the crystallization properties causing decrease of the interfacial free-energy, increase of nucleation rate, crystallization temperature, and decreases in scanning the spherulite size [21].

In this article, we report the effects of clay platelets and compatibilizer on the nanocomposites structure in terms of clay dispersion in polymer matrix, morphology, and crystallization behavior. Isotactic polypropylene/organo-modified layered silicate nanocomposites were prepared via single-step melt-mixing procedure, using PP-*g*-MA as compatibilizer, and the composites were analyzed by wide-angle X-ray diffraction (WAXD), scannig/transmission electron microscopy (SEM/TEM), polarizing optical microscopy (POM), and differential scanning calorimetry (DSC). Our previous investigation of thermal behavior of these composites carried out by TG/DTG method [22] exposed significant difference between thermal and thermo-oxidative stabilities of the examined nanocomposites, due to the different degradation mechanisms taking place during heating. Significant prolongation of oxidation induction time (measured at 200 °C) for nanocomposites in the presence of even 1% organo-modified clay, has been found.

Experimental

Materials

The isotactic polypropylene (iPP) matrix used was a homopolymer (Borclean HB300BF, Borealis) with M_w = 608 kg mol^{-1}, MFI = 2.5 g/10 min (230 °C, 2.16 kg), and a density of 0.91 g cm^{-3} supplied from COST Action P12: WG3-Polymer Bank [23]. Maleic anhydride-grafted PP (PP-*g*-MA, with MA content = 0.6 wt%, MFI = 115 at 190 °C/2.16 kg and a density of 0.95 g cm^{-3}), supplied by Aldrich is used as compatibilizer for promoting exfoliation of the organoclay, Cloisite C93A (Southern Clay Products, Inc) with a CEC of 90 meq/100 g clay, organically modified with ternary ammonium salt.

Preparation of nanocomposites

The iPP nanocomposites were obtained by direct melt mixing of the components in recirculating co-rotating twin-screw micro-extruder with a volume of 5 cm^3, made by DSM (The Netherlands), at 190 °C and 300 rpm for 30 min. The clay concentrations of 1 and 3 wt% were used for C93A-based nanocomposites, and fixed concentration of 10 wt% PP-*g*-MA. Neat iPP, iPP/PP-*g*-MA, and iPP/PP-*g*-MA/C93A nanocomposites (PCN) were compression-molded in a Collin Press 300G at 180 °C for 2 min without any applied pressure. After this period, a pressure of 100 bars was applied for 3 min and fast cooled to room temperature by press plates containing coils for water. Films of 100–300 μm were produced for further analyses by WAXD, POM, SEM/TEM, and DSC.

Characterization methods

Wide-angle X-ray diffraction analysis was performed on a Rigaku D/Max-B diffractometer (Japan), equipped with nickel-filtered CuKα_1 ($\lambda = 1.54056$ Å) radiation source operated at 40 kV and 25 mA. Corresponding data were collected at step scan rates of 0.02 and 1° min^{-1} in the range 2θ = 1.1–27° for clay particles and nanocomposite samples. The measurements were made on samples prepared by compression molding. Analysis of the WAXD patterns was done using basic peak fitting with Gaussian–Lorentzian function after background subtraction. The crystallite's size, L_{hkl} of iPP and nanocomposites were calculated from the peak broadening according to the Scherrer equation [18]:

$$L_{hkl} = K\lambda/\beta_o \cos\theta \quad (1)$$

where L_{hkl} is crystallite size perpendicular to reflection plane (hkl) (nm), θ is Bragg angle, λ is wavelength of X-ray used (nm), β_o is half-high width of diffraction peaks

(rad), K is shape factor of crystallite size, $K = 0.9$. The total crystallinity was obtained as a ratio of the integrated intensities under the crystalline peaks (A_c) and the integrated total intensities ($A_a + A_c$).

Polarizing optical microscopy (POM) was performed using a Leitz Biomed microscope equipped with a hot-stage (−20/350 °C) and a photo camera (Nicon-800). Extremely thin slices (*ca.* 0.02 mm) were cut from compression molded samples, inserted between two microscope slides (18 × 18 mm), melted up to 205 °C, and kept at this temperature for 5 min to erase the thermal history of the sample. Then, the samples were cooled down to a given crystallization temperature, T_c and were allowed to crystallize isothermally. Photomicrographs of growing spherulites were taken at appropriate time intervals.

Transmission electron microscopy observation was performed on Tecnai 20 operated in bright-field mode at 200 kV. Ultrathin sections of the PP/clay nanocomposite samples with a thickness of approximately 90 nm stained with RuO_4 solution were prepared at room temperature using an ultramicrotome Reichert–Jung Ultracut E equipped with a diamond knife. The sections were transferred dry to carbon-coated Cu grids of 200 meshes.

Scanning electron microscopy of iPP/C93A nanocomposites was performed using a Quanta 3D FEG (Fei Co.) equipped with a field-emission gun. High vacuum conditions were applied, and a secondary electron detector was used for image acquisition. No additional sample treatment such as surface etching or coating with a conductive layer has been applied before surface scanning. Standard acquisition conditions for charge contrast imaging were used.

Differential scanning calorimetry analysis was performed under nitrogen using DSC-7 analyzer (Perkin Elmer). In isothermal regime, 5 mg of a sample was rapidly heated to 220 °C, and the molten state was held 10 min to erase the thermal history of the polymer. Then, the sample was cooled at the maximum rate (200 °C) to the given crystallization temperature (T_c), and crystallization was carried out until it was completed. After crystallization at predetermined temperature (T_c), the samples were reheated to reach the melting state at a range of 10 °C min^{-1} so that the melting temperature is determined. The equilibrium melting temperature, T_m^o, was determined by the Hoffman–Weeks equation [24]:

$$T_m = T_m^o(1 - 1/\gamma) + T_c/\gamma \quad (2)$$

where T_m^o is the equilibrium melting temperature, which signifies the kinetic driving force for crystallization of a crystallizable polymer, and γ is a constant which depends on the ratio of the final thickness of the crystalline lamellae at time t and the initial thickness.

Straight lines are obtained when the observed melting temperature are plotted against the crystallization temperature, T_c, and on observing the intersection of this line with a line having a slope equal to unity ($T_c = T_m$). Nonisothermal crystallization was carried out at different cooling rates, β (5–20 °C min^{-1}) to analyze the effects of clay on the crystallization kinetics.

Results and discussion

WAXD analysis

WAXD technique is usually used for studying the formation of nanocomposites structure by measuring clay interlayer spacing (d_{001}) from the 2θ position of the clay (001) diffraction peak in iPP matrix using Bragg's law. The results of WAXD patterns in the range $2\theta = 1.3$–10° for C93A, iPP/PP-*g*-MA/C93A nanocomposite, containing 1 and 3 wt% C93A, and iPP/C93A 1 wt% without PP-*g*-MA are shown in Fig. 1a. The X-ray diffraction analysis performed on the organically modified clay showed peak at $2\theta \sim 3.52°$ (curve a), corresponding to basal spacing of silicate galleries of 25.1 Å. In order to investigate the effect of compatibilizer (PP-*g*-MA) on the dispersion of clay layers in iPP matrix the diffractogram of iPP/C93A 1 wt% nanocomposite without PP-*g*-MA is also shown (Fig. 1a, curve d). It is clear that the presence of compatibilizer significantly improves their interaction with the matrix leading to better dispersion of the clay. As can be seen from curve d, the characteristic peak of C93A (see curve a), although still intensive, was shifted to a lower value of $2\theta \sim 2.84°$, indicating the increase of clay basal spacing due to intercalation of polymer chains into silicate galleries. Similar behavior has been found in melt-mixed iPP/Cloisite 15A system where the clay aggregates have been sheared off and broken down into large stacks; in the presence of PP-*g*-MA, a diffusion process was observed in addition to the shear effect [18].

The absence of clay diffraction peak in the samples with iPP/PP-*g*-MA matrix and 1 wt% C93A indicates possible clay exfoliation (curve b). This may be a result of strong interaction between polar groups of PP-*g*-MA molecules and the silicate layer. Similar conclusions from the results of WAXD investigations based on similar traces have been drawn by other research groups [25]. In nanocomposite with 3% C93A (curve c) containing maleic anhydride, WAXD curve showed the presence of a broader diffraction peak appearing at higher 2θ-value, although the main clay peak disappeared. Considering the position of this peak, a possible coalescence of clay platelets can be supposed. It is possible that during processing, either some alkyl chains of surfactant have been degraded, or that chemical reaction between the surfactant and one of the components of the composites has proceeded [25], and as a result, the interlayer spacing has become lower [26].

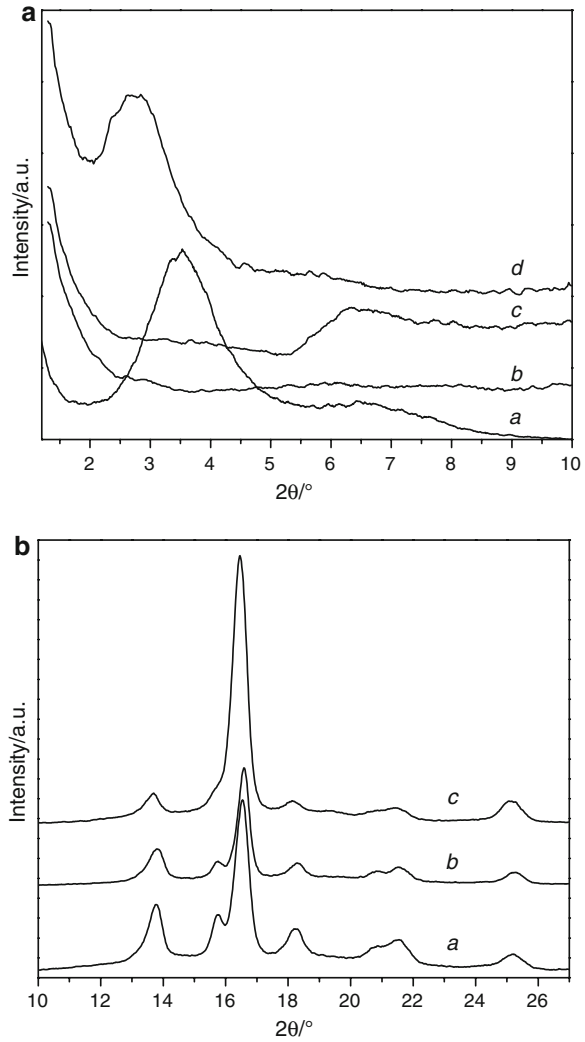

Fig. 1 WAXD patterns of **a** Cloisite C93A (*a*), iPP/PP-*g*-MA/C93A 1 wt% (*b*), iPP/PP-*g*-MA/C93A 3 wt% (*c*), and iPP/C93A 1 wt% (without PP-*g*-MA) (*d*) nanocomposite in the range $2\theta = 1$–10°, **b** neat iPP (*a*), iPP/PP-*g*-MA/C93A 1 wt% (*b*), and iPP/PP-*g*-MA/C93A 3 wt% (*c*) in the range $2\theta = 10$–27°

From the above mentioned, it should be concluded that WAXD patterns indicate the formation of possible exfoliated structure of nanocomposites containing 1 wt% clay, and mixed intercalated/exfoliated structure at higher concentration of nanoclay (3 wt% clay).

The effect of PP-*g*-MA and clay on the crystalline morphology of iPP as evaluated by WAXD in the 2θ range of 10–27° is presented in Fig. 1b. As shown in this figure, significant difference in relative intensities of the peaks α (110) and α (040) for the neat iPP matrix and the nanocomposites containing 1 and 3 wt% C93A was observed, but the peak position of the crystal planes did not shift with addition of C93A. This indicates that the typical pattern of α-crystalline iPP is not significantly affected by the presence of nanoclay. The characteristic reflection peak at $2\theta \sim 15.77°$ in the matrix iPP and nanocomposite sample (1 wt% clay) corresponds to the (300) reflection of β-iPP [27]. Investigation of the peculiarities of crystalline morphology of iPP (the weak β nucleation effect of iPP) in the presence of higher amount of C93A (disappearance of the characteristic peak for iPP at $2\theta \sim 15.77°$ and, correspondingly, appearance of a shoulder peak for nanocomposite containing 3 wt% C93A at the same 2θ) will be a subject of our further investigation. However, the presence of clay particles has probably resulted in the change of spatial confinement of the silicate layers, which significantly affects different crystallization ability of the matrix PP, and development of certain content of β-PP in the nanocomposite [28]. The results of WAXD analysis of neat iPP and nanocomposites are given in Table 1.

Table 1 Crystallite's size and overall crystallinity of iPP and iPP/PP-*g*-MA/C93A nanocomposites

Sample	L_{110}/nm	L_{040}/nm	L_{130}/nm	X_c/%
Neat iPP	11.1	14.0	15.5	62.4
iPP/PP-*g*-MA/C93A (1 wt%)	11.4	14.6	15.5	62.7
iPP/PP-*g*-MA/C93A (3 wt%)	12.5	14.6	15.5	69.1

As can be seen from Table 1, crystallite's sizes perpendicular to the crystal planes (110) and (040) in nanocomposites are slightly increased, whereas unchanged values are calculated for (130) crystal plane. For nanocomposite containing 3 wt% C93A, the value of the overall degree of crystallinity is increased by ~10% when compared to the neat iPP.

Polarized optical microscopy was used to compare the crystal morphology of PP nanocomposites developed during isothermal crystallization at various T_c. All the nanocomposite samples, as well as iPP/PP-*g*-MA (Fig. 2), were found to crystallize into spherulitic morphology similar to that of neat iPP, exhibiting a typical Maltese cross extinction [29]. However, the first visible nuclei of iPP/PP-*g*-MA appearing in the initial stage of growth are beanlike (Fig. 2a). Also, it was observed that the nucleation density decreases as T_c increased from 118 to 130 °C, in agreement with kinetic theory of crystallization [30, 31].

When spherulites nucleated at the beginning of crystallization in nanocomposite film reach considerable size, new spherulites are suddenly nucleated in the melt between them. Thus, the system consists of two different populations: one composed of large spherulites nucleated in the beginning of crystallization and other—of small spherulites nucleated later. As a result of this, at the end of crystallization voids are formed (Fig. 2c).

Morphological analysis by SEM/TEM

SEM micrographs of iPP/PP-*g*-MA/C93A 1 and 3 wt% nanocomposite samples at different magnification are

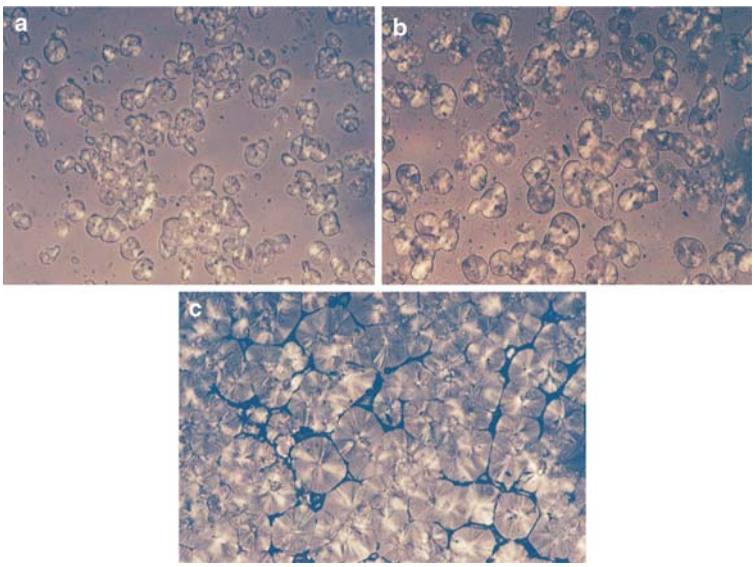

Fig. 2 POM micrographs of iPP/PP-*g*-MA (**a**), PP/PP-*g*-MA/C93A nanocomposite 3 wt% (**b**, **c**) crystallized isothermally at 124 °C (magnification 200×)

shown in Fig. 3a, b. It is evident that for nanocomposite sample with 1 wt% C93A, there is no contrast between clay and iPP matrix, which indicates the absence of particularly big aggregates (Fig. 3a). On the contrary, in nanocomposite with 3% C93A an aggregation is seen from SEM micrographs, thus confirming an assumption obtained from WAXS analysis (existence of mixed intercalated/exfoliated structure). The appearance of holes visible in some regions of the both nanocomposite samples might be an indication on good interfacial adhesion achieved between clay layers and maleic anhydride-modified iPP matrix.

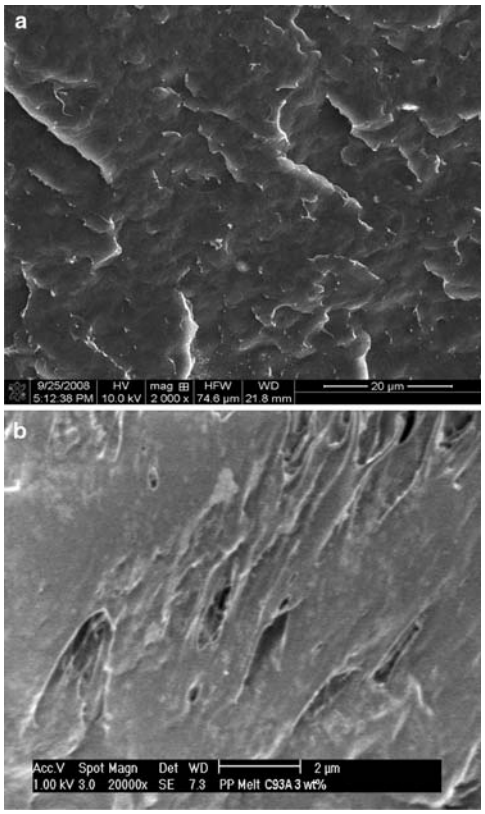

Fig. 3 SEM micrographs of iPP/PP-*g*-MA/C93A nanocomposites with 1 wt% (**a**) and 3 wt% clay (**b**) at different magnification 2000 and 20000×, respectively

Transmission electron microscopy supplements the WAXD and SEM techniques by the direct observation of the state of dispersion of clay platelets in the composites, since WAXD and SEM cannot provide complete information regarding the microstructure formation and the dissemination of clay particles inside the iPP matrix. Figure 4 shows the bright-field TEM micrographs of clay particles C93A in iPP/PP-*g*-MA matrix at clay loading of 1 wt%, at low and high magnification (Fig. 4a, b). The dark areas in TEM images represent the clay particles and the gray ones the continuous iPP matrix. As can be seen, fine and homogeneous dispersion of the clay is achieved (a), and transcrystalline organization of iPP lamellae in the sample with 1 wt% C93A is clearly evident (b). The bands correspond to the iPP crystal lamellae and can be seen to have much higher density around the nucleating clay layers than in the polymer-rich area, and extending in various directions without preferential orientation. Zheng et al. [32] reported that at lower clay contents, when clay is well exfoliated, the clay layers can be easily oriented with compression because of their large aspect ratio. However, when clay content is higher, the clay orientation is more difficult because of the reduced aspect ratio of clay, which would lead to more isotropic arrangement of PP crystallites.

The subject of transcrystallinity has also been addressed for nanocomposite systems based on nylon-6 [33], polyethylene [34, 35], poly(vinyl alcohol) [36], and other semicrystalline polymers showing that it might well

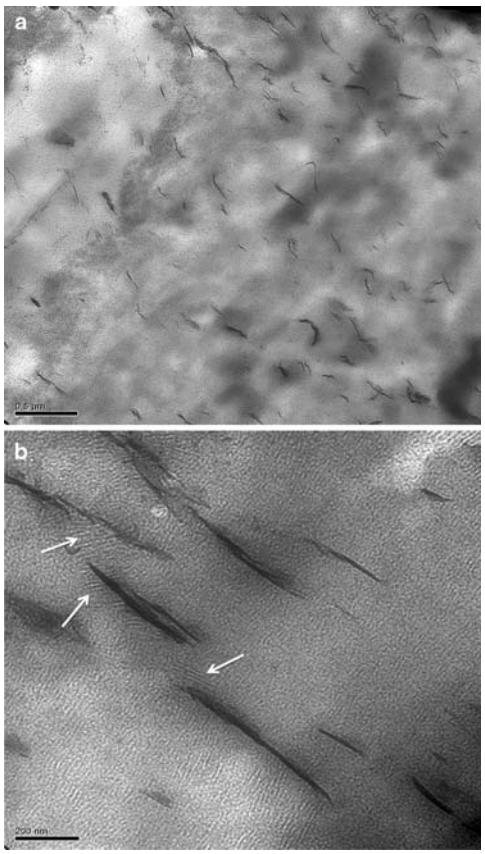

Fig. 4 TEM bright-field micrograph of iPP/PP-*g*-MA/C93A (1 wt%) nanocomposites at different magnification (**a**, **b**). *White arrows* indicate the presence of transcrystalline organization of the PP lamellae with different orientation around the clay layers

concern a general phenomenon rather than being restricted to a few specific matrix materials. For this reason, and in view of the extremely high specific surface area provided by the nanofillers, the formation of an ordered crystalline interface may also be of prime important technological relevance, as it was, for instance, recognized that the nature of the interface plays a fundamental role in the reinforcement mechanism [37, 38].

The overall nanocomposite morphology can be regarded as a multiphase structure, consisting of individually dispersed filler particles, and a surrounding transcrystalline interphase in which polymer chains display a reduced segmental mobility. This conclusion is derived based on the investigation of glass transition temperature (T_g) of nanocomposites, derived as a maximum of the transition tan δ versus temperature during dynamic mechanical analysis carried out in tension mode in the temperature range from −50 to 150 °C. The decreased value of T_g (8.1 °C) of iPP matrix for sample containing 1 wt% of C93A compared to neat iPP (12.1 °C) is in agreement with the fact that the addition of clay particles influences the mobility of polymer chains [39].

DSC isothermal crystallization

For a better understanding of the interaction between clay particles and the surrounding iPP/PP-*g*-MA matrix, we have performed DSC isothermal crystallization experiments carried out in the temperature range of T_c = 118–130 °C. Crystal conversions of the neat iPP, iPP/PP-*g*-MA, and iPP/PP-*g*-MA/C93A nanocomposites were determined, and the results for T_c = 127 °C are presented in Fig. 5. From Fig. 5, one can see that the isothermal crystallization of the matrix polymer (iPP/PP-*g*-MA) proceeds faster than in the nanocomposite samples. For the investigated samples. a similar behavior was also found in the whole T_c's range. The presence of PP-*g*-MA in a matrix polymer has enhanced the crystallization, and this is in agreement with our previous results, in which an improved nucleation ability of iPP, containing even significantly lower content of PP-*g*-MA, was found as a consequence of reduced critical dimensions of growing nuclei, the effect being ascribed to the presence of carbonyl groups in the polymer backbone [29, 40, 41].

Many reports of iPP/PP-*g*-MA/clay nanocomposites have appeared in the literature showing the effect of the clay intercalation/exfoliation on the crystallization behavior [7, 19, 42], and they are, often, still controversial. Most researchers [43, 44] observed an increase in crystallization rate, while other groups reported that the filler slowed it down [45], or had no effect [46] on the kinetics. Svoboda et al. [7] found that acceleration of isothermal crystallization proceeds only in nanocomposite systems containing the clay tactoids (intercalated system), while no nucleation ability of montmorillonite (MMT) was found in systems with exfoliated clay. Similar results were reported by Kim et al. [42] who observed an increase in the crystallization

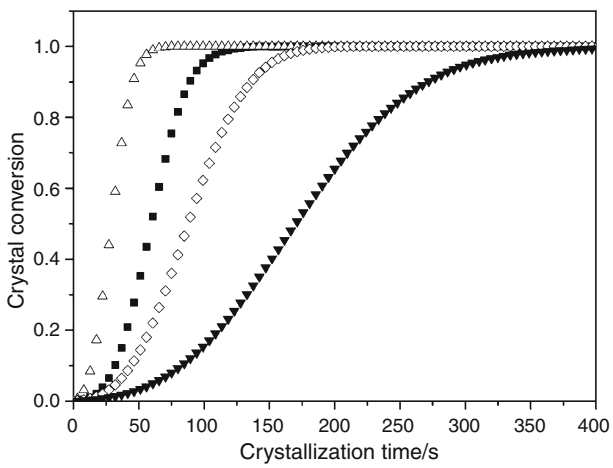

Fig. 5 Crystal conversion curves of the iPP (*filled square*), iPP/PP-*g*-MA (*open triangle*), iPP/PP-*g*-MA/C93A 1% (*open diamond*), and iPP/PP-*g*-MA/C93A 3% (*inversted closed triangle*) nanocomposites crystallized at T_c = 127 °C

rate for agglomerated/intercalated systems, while exfoliated nanocomposites crystallized more slowly than neat polymer. This was ascribed not only to a diffusion barrier enacted by clay layers, but also to the release of the organic modifier that might hinder crystallization.

The DSC melting behavior at a heating rate of 10 °C min^{-1} of isothermally crystallized samples was investigated. Figure 6 shows the melting traces for the iPP nanocomposites containing 1 and 3 wt% C93A and iPP/PP-*g*-MA matrix, respectively.

The presence of clay particles did not induce significant changes in melting behavior of the matrix after isothermal crystallization at given T_c showing no shift in the melting temperature. In nanocomposite samples, a weak melting shoulder (more pronounced at lower clay loading) can be observed at ~150 °C, indicating the presence of small amount of β-modification of iPP, previously confirmed by the weak reflection peak (300) in WAXD results (Fig. 1b). The obtained values of full width at half-high (ΔW) of melting peak (melting after isothermal crystallization carried out in temperature range from 118 to 130 °C) of iPP/PP-*g*-MA are higher compared to those of neat iPP, suggesting the broader distribution of the crystal dimensions. However, for nanocomposite samples, a decrease of ΔW compared to those of the matrix was determined, suggesting more uniform distribution of the crystal's dimensions caused by the presence of the clay.

Furthermore, the degree of crystallinity, calculated from the enthalpy of melting ($\Delta H_m = 104$ and 105 J g^{-1} for nanocomposites containing 1 and 3 wt% C93A, respectively) compared to that of neat iPP ($\Delta H_m = 104$ J g^{-1}), remains practically unchanged with the addition of clay.

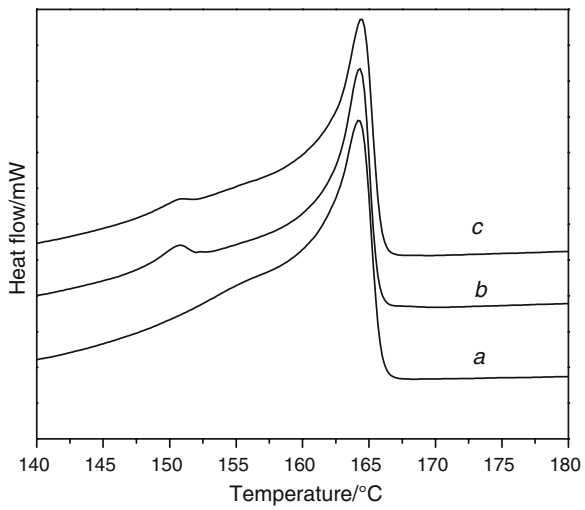

Fig. 6 Melting curves of the iPP/PP-*g*-MA (*a*), iPP/PP-*g*-MA/C93A 1% (*b*), and iPP/PP-*g*-MA/C93A 3% (*c*) nanocomposites after isothermal crystallization at $T_c = 127$ °C

This is not particularly surprising, since nucleating agents actually do not affect crystallinity to a large extent.

The melting temperatures T_m as a function of crystallization temperatures T_c for neat iPP and the iPP/PP-*g*-MA/clay nanocomposites are reported in Fig. 7. The values of T_m^o and γ constant were calculated by extrapolation of the T_m versus T_c line to the line of equation $T_m = T_c$ and from the slope. The obtained values of T_m^o and γ constant are shown in Table 2.

As can be seen from Table 2, the T_m^o value for iPP/PP-*g*-MA sample decreases compared with neat iPP, indicating an increase of the number of defects between iPP lamellae which appeared with the presence of MA groups. For nanocomposites, the addition of clay has resulted in similar values for T_m^o compared with neat PP but slightly higher compared to iPP/PP-*g*-MA, suggesting that T_m^o depends predominantly on the matrix material. This phenomenon might result from the nucleation effect of the clay, confirmed also by the lower values of γ constant found for the both composites.

The literature data for the equilibrium melting temperatures of iPP differ and are in the range from 185 to

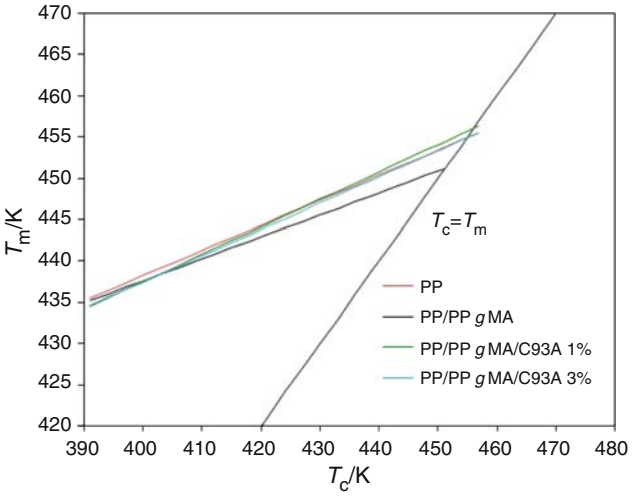

Fig. 7 Melting temperatures, T_m as a function of crystallization temperature, T_c for iPP, iPP/PP-g-MA, and its nanocomposites (1 and 3 wt% clay)

Table 2 Equilibrium melting temperatures, T_m^o and γ constant calculated for neat iPP, iPP/PP-*g*-MA, and nanocomposites

Sample	T_m^o/°C	γ
Neat iPP	182	3.3
iPP/PP-*g*-MA	178	3.8
iPP/PP-*g*-MA/C93A (1 wt%)	183	3.0
iPP/PP-*g*-MA/C93A (3 wt%)	182	3.4

208 °C for α iPP with high isotacticity content [47]. Lower values of T_m^o and higher for γ constant for iPP in glass–fiber composites as the content of fibers increases were also observed, indicating that increasing the filler content increases the number of defects between iPP lamellae [29]. A decrease of T_m^o by addition of MMT in nanocomposite systems containing clay tactoids was found by Svoboda et al. [7]. Kim et al. [42], and Causin et al. [19] reported that both exfoliated and intercalated nanocomposite systems were found to depress the T_m^o. Maiti et al. [46] investigated intercalated PP-*g*-MA/OMMT nanocomposites and found that OMMT has no effect on T_m^o. An increase in T_m^o of exfoliated PP/clay nanocomposites with respect to neat iPP was reported by Ma et al. [43].

Non-isothermal crystallization

The DSC scans recorded during nonisothermal crystallization of investigated samples at cooling rates from 5 to 20 °C min^{-1} are given in Fig. 8. The obtained results represent an evidence for a pronounced nucleation effect of the clay: the crystallization from the melt of the system containing 1% clay starts at higher temperatures as compared to the matrix PP. The prominent formation of the transcrystalline layer of iPP around clay platelets (see Fig. 3b) in this system obviously demonstrates its potential as nucleation agent.

Nucleating effect is more pronounced in nanocomposite samples with 1% clay as compared to the one with 3% clay, probably as a result of the increased interfacial area, characteristic for exfoliated (1%) rather than mixed intercalated/exfoliated system (3%).

As shown in Fig. 8a, the addition of 1 wt% clay into PP matrix causes the crystallization onset temperature ($T_{c,onset}$) to increase from 127.7 to 129 °C (at cooling rate of 5 °C min^{-1}), while no significant changes were observed at higher clay content.

Similar tendency was also obtained for the higher cooling rates of 10 and 20 °C min^{-1} (see Fig. 8b, c, respectively). The fact that crystallization onset and peak temperatures level off at higher clay content (3 wt% clay) is indicative of some degree of nucleation saturation as a result of an incomplete exfoliation implying that much of outer surface of clay is inaccessible for crystal nucleation. Saturation of the nucleating effect was observed for PP/CNT (2 wt%) nanocomposites and was attributed to agglomeration of the nucleating particles [37].

The increase in crystallization temperature of about 5 °C with addition of 3–5 wt% organo-modified clay was

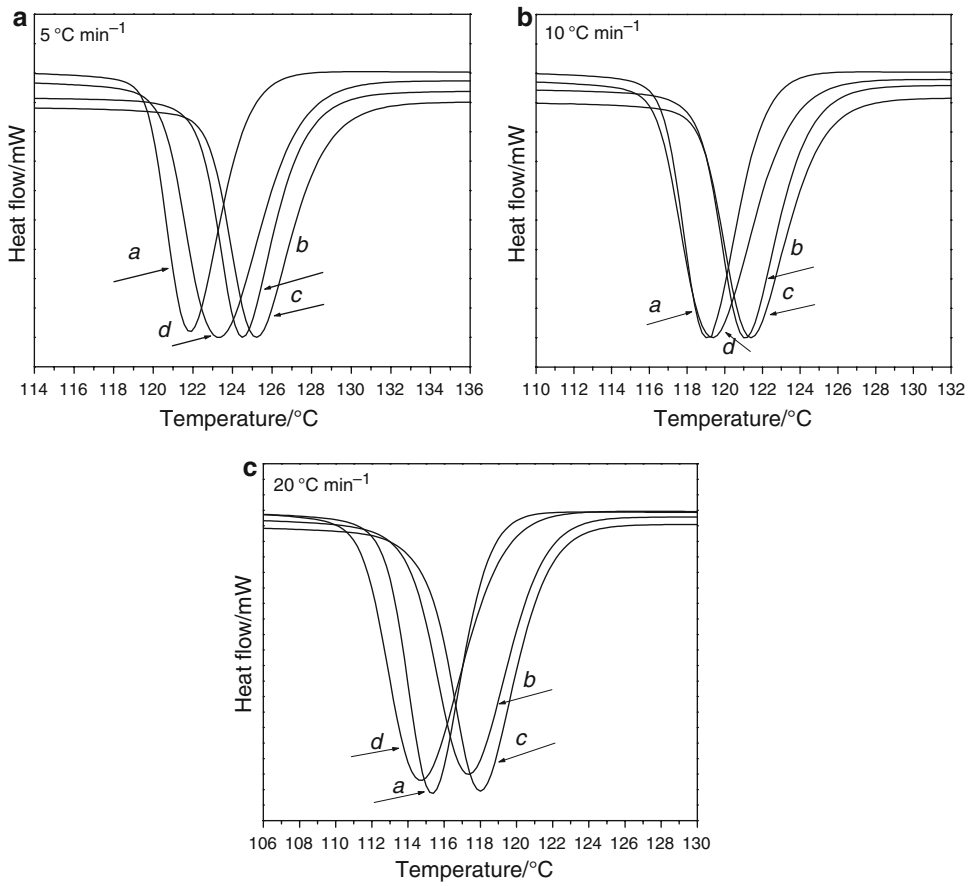

Fig. 8 DSC patterns of neat iPP (*a*), iPP/PP-*g*-MA (*b*), iPP/PP-*g*-MA/C93A 1 wt% (*c*), and iPP/PP-*g*-MA/C93A 3 wt% (*d*) nanocomposites during crystallization from quiescent melt (at cooling rates 5, 10, and 20 °C min^{-1})

also reported by other authors [46, 48, 49]. Xu et al. [48] found higher crystallization temperature for PP/PP-*g*-MA/O-MMT system than that of pure PP, which is explained in terms of interactions between the carboxyl group of PP-*g*-MA and clay particles. A number of studies have reported that the role of compatibilizer in crystallization kinetics of PP is likely to be minor, because increase of crystallization rate has been observed both for compatibilized and non-compatibilized systems [19, 45]. Perrin-Sarazin et al. [17] noted that the kinetics of crystallization is not only related to the clay content, but also depends on PP–clay interactions: in the absence of the coupling agent, the crystallization of PP occurred at higher temperature and at a higher rate than neat PP, but the crystallization behavior was similar to neat PP when coupling agent was added. Nowacki [50] suggested that only weak nucleating ability of clay is expected during crystallization in quiescent condition, which is greatly enhanced during shear-induced crystallization.

From the obtained curves, additional parameters, such as the initial slope of the exotherm at inflection on the high-temperature side, S_i, and the full width at half height of the exothermic peak, ΔW could be obtained for describing the nonisothermal crystallization kinetics [51]. Based on these parameters, the crystallization of neat iPP and iPP/PP-*g*-MA at 5 °C min^{-1} seems to be faster ($S_i = 6.31$ and 5.14 a.u., respectively) than that of the nanocomposites ($S_i = 4.7$ and 4.3 a.u., for 1 and 3 wt% C93A, respectively), although it starts at higher temperature (earlier) for the nanocomposite with 1% of clay.

The ΔW refers to the distribution of the forming crystal dimensions; i.e., the smaller the ΔW, the narrower the distribution. As we can see from Table 3, ΔW increases with addition of nanoclay particles, which suggests the broader distribution of the crystal dimensions in both nanocomposite samples. It is also evident that the values of ΔW are affected by the cooling rate: lower values of ΔW are obtained during crystallization at lower cooling rates, with addition of PP-*g*-MA and clay for all samples, indicating the narrower distribution of the crystal dimensions (Table 3).

According to our results, it could be concluded that when clay was exfoliated, the effect was more pronounced (the crystallization from the quiescent melt for nanocomposite with 1 wt% C93A starts at higher temperatures compared to that of iPP/PP-*g*-MA) with respect to that of mixed intercalated/exfoliated system (nanocomposite with 3 wt% C93A). It seems reasonable to assume that the extent of the effect of polymer/clay interface on the crystallization behavior is strongly linked to the interfacial region between polymer and filler.

It should be mentioned, that the morphology of nanocomposites plays an important role in their thermal stability, as measured by TGA: significant prolongation of oxidation induction time (isothermal treatment at 200 °C in air atmosphere) in polypropylene nanocomposites in the presence of even 1% organo-modified clay (exfoliated structure) compared to ones with 3 wt% clay (intercalated/exfoliated structure) was observed. The difference in induction time determined for these nanocomposites is likely related to the different degree of dispersion of nanofiller, as it was shown in our previous investigation [22].

Table 3 ΔW of the crystallization peak during nonisothermal crystallization of the matrix polymer and nanocomposites

Sample	5 °C min^{-1}	10 °C min^{-1}	20 °C min^{-1}
PP	3.18	3.25	3.71
PP/MAH	3.36	3.81	4.33
PP/MAH/C93A 1 wt%	3.74	4.08	4.65
PP/MAH/C93A 3 wt%	4.39	4.42	4.79

The melting behavior after nonisothermal crystallization was found to be affected by the presence of clay particles (Fig. 9). After crystallization at the same cooling rate, the melting endotherms with addition of PP-*g*-MA and C93A become broader, indicating on broader distribution of the formed crystal dimensions.

Nonisothermal crystallization experiments generally confirm the conclusion of isothermal crystallization experiments: the addition of clay seems to decrease the degree of crystallinity (especially at higher cooling rates) as a result of low nucleating effect of clay platelets.

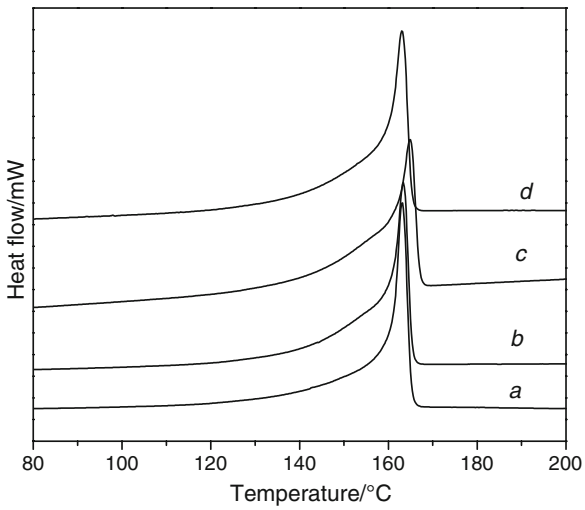

Fig. 9 Melting curves of neat iPP (*a*), iPP/PP-*g*-MA (*b*), iPP/PP-*g*-MA/C93A 1% (*c*), and iPP/PP-*g*-MA/C93A 3%, (*d*) nanocomposites after nonisothermal crystallization at 5 °C min^{-1}

Conclusions

Polypropylene nanocomposites with organo-modified layered silicate (C93A) and PP-*g*-MA as compatibilizer were prepared by single-step melt-mixing procedure. The effects of clay platelets and compatibilizer on the nanocomposite structure in terms of clay dispersion in iPP matrix, morphology, and crystallization behavior were studied. The obtained results have shown that single-step mixing procedure leads to iPP nanocomposites with homogeneous dispersion of organo-modified clay. WAXD patterns, showing a small amount of β modification of iPP, revealed exfoliated structure of nanocomposites containing 1 wt% C93A, and mixed intercalated/exfoliated structure at higher clay concentration (3 wt%). As confirmed by WAXD and SEM analyses, the degree of intercalation/exfoliation was improved by the addition of 10 wt% compatibilizator (PP-*g*-MA). Investigation carried out by TEM technique revealed existence of differently oriented transcrystalline structures of polymer lamellae around clay layers. The nanocomposites as well as iPP/PP-*g*-MA were found to crystallize into spherulitic morphology similar to that of neat iPP. The isothermal crystallization proceeds faster in the matrix polymer (iPP/PP-*g*-MA) than in nanocomposite samples. The results obtained for T_m^o suggest that the presence of nanoclay has induced a perfection of the formed crystals. During nonisothermal crystallization the presence of C93A particles in iPP leads to increase in crystallization peak temperature at a given cooling rate implying a pronounced nucleating ability of clay particles. This effect was more pronounced in exfoliated than in mixed intercalated/exfoliated system.

Acknowledgements The financial support from COST Action P12 "Structuring of Polymers," COST-STSM-P12-02842 is greatly appreciated. Thanks are due to the Ministry of Education and Science of Republic of Macedonia for the financial support of the COST-related project activities. We thank Dr. Kangbo Lu from the Department of Chemical Engineering and Chemistry, Eindhoven University of Technology for TEM measurements.

References

1. Mülhaupt R, Stricker F. PP-compounds als konstruktionswerkstoffe: Eigenschaften der PP-compounds bei einsatz von mikro-bzw. Nanofüllstoffen = PP compounds as engineering materials. Kunststoffe. 1997;87:482–6.
2. Giannelis EP. Polymer layered silicate nanocomposites. Adv Mater. 1996;8:29–35.
3. Pinnavaia TJ, Lan T, Wang Z, Shi H, Kaviratna PD. Clay-reinforced epoxy nanocomposites: synthesis, properties, and mechanism of formation. In: Chow GM, Gonsalves KE, editors. Nanotechnology, vol. 622. ACS Symp Ser. Washington: American Chemical Society; 1996. p. 251.
4. Reichert P, Nitz H, Klinke S, Brandsch R, Thomann R, Mülhaupt R. Poly(propylene)/organoclay nanocomposite formation: influence of compatibilizer functionality and organoclay modification. Macromol Mater Eng. 2000;275:8–17.
5. Zanetti M, Lomakin S, Camino G. Polymer layered silicate nanocomposites. Macromol Mater Eng. 2000;279:1–9.
6. Ray SS, Okamoto M. Polymer/layered silicate nano-composites: a review from preparation to processing. Prog Polym Sci. 2003; 28:1539–641.
7. Svoboda P, Zeng C, Wang H, Lee LJ, Tomasko DL. Morphology and mechanical properties of polypropylene/organoclay nanocomposites. J Appl Polym Sci. 2002;85:1562–70.
8. Alexsandre M, Dubois P. Polymer-layered silicate nanocomposites: preparation, properties and use of a new class of materials. Mater Sci Eng. 2000;28:1–63.
9. Grossiord N, Loos J, Koning CE. Strategies for dispersing carbon nanotubes in highly viscous polymers. J Mater Chem. 2005;15: 2349–52.
10. Regev O, El Kati PNB, Loos J, Koning CE. Preparation of conductive nanotube-polymer composites using latex technology. Adv Mater. 2004;16(3):248–51.
11. Wang K, Xiao Y, Na B, Tan H, Zhang Q, Fu Q. Shear amplification and re-crystallization of isotactic polypropylene from an oriented melt in presence of oriented clay platelets. Polymer. 2005;46:9022–32.
12. Varela C, Rosales C, Perera R, Matos M, Poirier T, Blunda J, et al. Functionalized polypropylenes in the compatibilization and dispersion of clay nanocomposites. Polym Compos. 2006;27:451–60.
13. Giannelis EP, Krishnamoorti R, Manias E. Polymer-silicate nanocomposites: model systems for confined polymers and polymer brushes. Adv Polym Sci. 1999;138:107–47.
14. Kawasumi M, Hasegawa N, Kato M, Usuki A, Okada A. Preparation and mechanical properties of polypropylene–clay hybrids. Macromolecules. 1997;30:6333–8.
15. Ma XY, Liang GZ, Liu HL, Fei JY, Huang Y. Novel intercalated nanocomposites of polypropylene/organic-rectorite/polyethylene-octene elastomer: rheology, crystallization kinetics, and thermal properties. J Appl Polym Sci. 2005;97:1915–21.
16. Avella M, Cosco S, Di Lorenzo ML, Di Pace E, Errico ME. Influence of $CaCO_3$ nanoparticles shape on thermal and crystallization behavior of isotactic polypropylene based nanocomposites. J Therm Anal Calorim. 2005;80:131–6.
17. Perrin-Sarazin F, Ton-That MT, Bureau MN, Denault J. Micro- and nano-structure in polypropylene/clay nanocomposites. Polymer. 2005;46:11624–34.
18. Ton-That MT, Perrin-Sarazin F, Cole KC, Bureau MN, Denault J. Polyolefin nanocomposites: formulation and development. Polym Eng Sci. 2004;44:1212–9.
19. Causin V, Marega C, Saini R, Marigo A, Ferrara G. Crystallization behavior of isotactic polypropylene based nanocomposites. J Therm Anal Calorim. 2007;90:849–57.
20. Menyhárd A, Faludi G, Varga J. Beta-crystallisation tendency and structure of polypropylene grafted by maleic anhydride and its blends with isotactic polypropylene. J Therm Anal Calorim. 2008;93:937–45.
21. Wang K, Xiao Y, Na B, Tan H, Zhang Q, Fu Q. Shear amplification and re-crystallization of isotactic polypropylene from an oriented melt in presence of oriented clay platelets. Polymer. 2005;46:9022–32.
22. Bogoeva-Gaceva G, Raka L, Dimzoski B. Thermal stability of polypropylene/organo-clay nanocomposites produced in a single-step mixing procedure. Adv Comp Lett. 2008;17(5):161–4.
23. COST P12 Action. In: Bank of crystallisable polymers, "structuring of polymers". 2006. Available via DIALOG. http://www.unirostock.de/fakult/manafak/physik/poly/COST_P12/.
24. Hoffman JD, Weeks JJ. Melting process and the equilibrium melting temperature of polychlorotrifluoroethylene. J Res Natl Bur Stand A. 1962;66A:13–28.

25. Százdi L, Ábrányi Á, Pukánszky B, Vancso GJ. Morphology characterization of PP/clay nanocomposites across the length scales of the structural architecture. Macromol Mater Eng. 2006; 291:858–68.
26. Modesti M, Lorenzetti A, Bon D, Besco S. Effect of processing conditions on morphology and mechanical properties of compatibilized polypropylene nanocomposites. Polymer. 2005;46: 10237–45.
27. Varga J. Beta-modification of isotactic polypropylene: preparation, structure, processing, properties, and application. J Macromol Sci. 2002;B41:1121–71.
28. Tang XG, Yang W, Bao RY, Shan GF, Xie BH, Yang MB, et al. Effect of spatial confinement on the development of beta phase of polypropylene. Polymer. 2009;50:4122–7.
29. Janevski A, Bogoeva-Gaceva G, Mäder E. DSC analysis of crystallization and melting behavior of polypropylene in model composites with glass and poly(ethylene terephthalate) fibers. J Appl Polym Sci. 1999;74:239–46.
30. Avella M, Cosco S, Della Volpe G, Errico ME. Crystallization behavior and properties of exfoliated isotactic polypropylene/ organoclay nanocomposites. Adv Polym Technol. 2005;24: 132–44.
31. Bogoeva-Gaceva G, Janevski A, Mäder E. Characterization of a maleic anhydride-modified polypropylene as an adhesion promoter for glass fiber composites. J Adhes Sci Technol. 2000;14: 363–80.
32. Zheng J, Lu X, Toh CL, Zheng TH, He C. Effects of clay on polymorphism of polypropylene in polypropylene/clay nanocomposites. J Polym Sci B. 2004;42:1810–6.
33. Dasari A, Yu Z, Mai YW. Transcrystalline regions in the vicinity of nanofillers in polyamide-6. Macromolecules. 2007;40:123–30.
34. Haggenmueller R, Fischer JE, Winey KI. Single wall carbon nanotube/polyethylene nanocomposites: nucleating and templating polyethylene crystallites. Macromolecules. 2006;39:2964–71.
35. Trujillo M, Arnal ML, Muller AJ, Laredo E, Bredeau S, Bonduel D, et al. Thermal and morphological characterization of nanocomposites prepared by in situ polymerization of high-density polyethylene on carbon nanotubes. Macromolecules. 2007;40: 6268–76.
36. Cadek M, Coleman JN, Ryan KP, Nicolosi V, Bister G, Fonseca A, et al. Reinforcement of polymers with carbon nanotubes: the role of nanotube surface area. Nano Lett. 2004;4:353–6.
37. Miltner HE, Grossiord N, Lu K, Loos J, Koning CE, Van Mele B. Isotactic polypropylene/carbon nanotube composites prepared by latex technology. Thermal analysis of carbon nanotube-induced nucleation. Macromolecules. 2008;41:5753–62.
38. Lu K, Grossiord N, Koning CE, Miltner HE, Van Mele B, Loos J. Carbon nanotube/isotactic polypropylene composites prepared by latex technology: morphology analysis of CNT-induced nucleation. Macromolecules. 2008;41(21):8081–5.
39. COST Action P12. 2006. "Structuring of polymers", COST-STSM-P12-02842. Scientific report. http://www.unirostock.de/fakult/manafak/physik/poly/COST_P12/.
40. Bogoeva-Gaceva G, Janevski A, Mäder E. Characterization of a maleic anhydride-modified polypropylene as an adhesion promoter for glass fiber composites. J Adhes Sci Technol. 2000;14: 363–80.
41. Bogoeva-Gaceva G, Janevski A, Mäder E. Nucleation activity of glass fibers towards iPP evaluated by DSC and polarizing light microscopy. Polymer. 2001;42:4409–16.
42. Kim B, Lee SH, Lee D, Ha B, Park J, Char K. Crystallization kinetics maleated polypropylene/clay hybrids. Ind Eng Chem Res. 2004;43:6082–9.
43. Ma J, Zhang S, Qi Z, Li G, Hu Y. Crystallization behaviors of polypropylene/montmorillonite nanocomposites. J Appl Polym Sci. 2002;83:1978–85.
44. Hambir S, Bulakh N, Jog JP. Polypropylene/clay nanocomposites: effect of compatibilizer on the thermal, crystallization and dynamic mechanical behavior. Polym Eng Sci. 2002;42:1800–7.
45. Somwangthanaroj A, Lee EC, Solomon MJ. Early stage quiescent and flow-induced crystallization of intercalated polypropylene nanocomposites by time-resolved light scattering. Macromololecules. 2003;36:2333–42.
46. Maiti P, Nam PH, Okamoto M, Hasegawa N, Usuki A. Influence of crystallization on intercalation, morphology, and mechanical properties of polypropylene/clay nanocomposites. Macromolecules. 2002;35:2042–9.
47. Varga J. Crystallization melting and supermolecular structure of isotactic polypropylene. In: Karger-Kocsis J, editor. Polypropylene: structure, blends and composites, vol. 1. London: Chapmann & Hall; 1995. p. 56–115.
48. Xu W, Liang G, Zhai H, Tang Sh, Hang G, Pan WP. Preparation and crystallization behaviour of PP/PP-g-MAH/Org-MMT nanocomposite. Eur Polym J. 2003;39:1467–74.
49. Xu W, Ge M, He P. Nonisothermal crystallization kinetics of polypropylene/montmorillonite nanocomposites. J Polym Sci B. 2002;40:408–14.
50. Nowacki R, Monasse B, Piorkowska E, Galeski A, Haudin JM. Spherulite nucleation in isotactic polypropylene based nanocomposites with montmorillonite under shear. Polymer. 2005;45: 4877–92.
51. Wang JL, Dong CM. Physical properties, crystallization kinetics, and spherulitic growth of well-defined poly(epsilon-caprolactone)s with different arms. Polymer. 2006;47:3218–28.